828 A Novel Approach To Reducing Dealiasing Errors For Staggered Pulse Repetition Time Waveforms

David A. Warde*[1,2], Adam Heck[3], Jane C. Krause[3,4], Autumn Losey[3], and W. David Zittel[3]
[1]Cooperative Institute for Mesoscale Meteorological Studies, The University of Oklahoma, Norman, OK
[2]NOAA/OAR National Severe Storms Laboratory, Norman, OK
[3]NOAA/NWS Radar Operations Center, Norman, OK
[4]Centuria Corporation, Norman, OK

ABSTACT

   Implementation, integration, and testing of staggered pulse repetition time (PRT) waveforms for improved range and velocity ambiguity mitigation is well underway for the NEXRAD network. The operational use of staggered PRT waveform is expected to replace the batch waveform used at intermediate levels of NEXRAD volume coverage patterns. Early analysis of staggered PRT output has shown improvement in the quality of reflectivity, spectrum width, differential reflectivity, cross-correlation coefficient, and differential phase over batch output. However, a major hindrance is the unexpected increase in dealiasing errors associated with the staggered PRT waveform. In this paper, we review the implementation and integration and provide some results of testing staggered PRT on the NEXRAD WSR-88D testbed. Additionally, we offer a novel approach to mitigating dealiasing errors associated with the staggered PRT waveform.

1. INTRODUCTION

   Range and velocity ambiguities at the intermediate elevation levels of operational volume coverage patterns (VCP) on the NEXRAD WSR-88D Network of S-band, Polarimetric Doppler weather radars are currently provided by batch waveforms (a holdover before the dual-polarimetric upgrade). In batch, 1-degree radials are formed by dividing the radial into two alternating sets of PRTs. The unambiguous range determination of reflectivity estimates for distant storms is provided by only a few pulses (typically $\leq$ 6 pulses) of a long PRT; while, the unambiguous velocity and spectrum width are provided by a larger number of pulses at a lower PRT. Since the quality of polarimetric estimates would not be operationally acceptable with the few pulses available in the long PRT, the estimates of differential reflectivity, cross-correlation coefficient, and differential phase are made using the lower PRT. Predictably, the low number of pulses in the long PRT cause the quality of reflectivity to suffer due to the ineffectiveness of clutter mitigation (which currently uses a 2-pulse canceller); and, the quality of the Doppler and polarimetric estimates suffer from range obscurations during widespread events as well as velocity aliasing during high wind events.

 *Corresponding Author Address: David A. Warde, CIMMS/University of Oklahoma, National Severe Storms Laboratory, National Weather Center, 120 David L. Boren Blvd. Norman, OK, 73072; David.A.Warde@noaa.gov

   To combat both range and velocity ambiguities at intermediate elevations, the Radar Operations Center (ROC) has implemented the 2/3 ratio staggered PRT waveform to replace the batch waveform. The basic staggered PRT algorithm (Torres et al. 2004) includes enhancements in range-overlay determination (Warde and Torres 2009), spectral processing (Torres and Warde 2014), clutter mitigation (Warde and Torres 2014), and spectrum width determination (Warde and Torres 2014, 2017, Meymaris and Hubbert 2015). To reduce so called 'catastrophic' velocity dealiasing errors associated with staggered PRT, augmented velocity dealiasing is provided by an enhanced NEXRAD velocity dealiasing algorithm (Torres et al. 2009). Recently, this processing step has come under scrutiny for its inability to properly handle velocity errors associated with staggered PRT. Several dealiasing issues were noted in regions that exhibited shear, storm top divergence, and weak echoes where the velocity field appeared noisier than the velocity fields from batch waveform processing. In this paper, we examine the dealiasing errors and provide a novel approach to mitigate these errors. First, we provide some results of testing staggered PRT on the NEXRAD WSR-88D testbed.

2. TESTING STAGGERED PRT

   Recently, testing of the staggered PRT implementation on the NEXRAD WSR-88D testbed has started. Data was collected using special test volume coverage patterns (VCP) such as VCP 51 (2/3 staggered PRT) and VCP 52 (batch) that operate at 0.5° and 0.9° elevations. These collection strategies were run sequentially to compare staggered PRT data quality to batch data quality with a small temporal difference (~1 minute). The lower elevations were chosen to test the clutter suppression capability of CLEAN-AP in staggered PRT; however, it should be noted that VCP 51 employs staggered PRT at elevations that are not recommended for operational use due the likelihood of excessive range-folded echoes. Even so, the acquisition parameters for staggered PRT are those recommended at intermediate elevations, so in the absence of range folded echoes, the performance of the staggered PRT algorithm using these experimental VCPs should be similar to what is expected operationally.
   Data from February 20, 2017 for the 0.9° elevation shown in Figs. 1 – 6 for VCP 52 (left panel, batch) and VCP 51 (right panel, staggered PRT) are representative of the types of comparisons done to evaluate the performance of staggered PRT with batch. It can be

seen that the quality of reflectivity (Fig. 1) using staggered PRT (right panel) is much improved over batch (left panel) by noting the variability and lack (e.g., holes in the data) of reflectivity values especially in weak signal regions (e.g., southwest of the radar in left panel compared to right panel). Moreover, the clutter suppression, provided by CLEAN-AP, is quite effective (50 dB of clutter suppression for this case). As for the polarimetric variables, differential reflectivity (Fig. 2), cross-correlation coefficient (Fig. 3), and differential phase (Fig. 4), no range-folded obscuration (purple color in figures) are observed when using staggered PRT as compared to using batch. That is, the polarimetric variables in staggered PRT can be recovered without range-overlaid echoes similarly to reflectivity (e.g., Torres et al. 2004, Warde and Torres 2009). Note that the incorrect values in the cross-correlation coefficient (Fig. 3, right panel, blue arrow) and spectrum width (Fig. 5, right panel, blue arrow) in staggered PRT beyond the unambiguous range of the short PRT were discovered and corrected after analyzing this data. Furthermore, the spectrum width estimates, shown in Fig. 5, were not compared due to a difference in processing. Specifically, the batch field is estimated using the NEXRAD hybrid spectrum width estimator (Meymaris et al. 2009); whereas the staggered PRT field is estimated using only the R0/R1 estimator. However, a hybrid spectrum width estimator is currently being developed and tested for use in staggered PRT (Meymaris and Hubbert 2015). The velocity field for this case is shown in Fig. 6. The unambiguous velocity of 28.5 m s^{-1} (55.4 knots) for batch (left panel) causes some aliasing to occur in the storms to the southwest of the radar; conversely, the unambiguous velocity of 37.1 m s^{-1} (72.1 knots) for staggered PRT (right panel) provides proper dealiasing these storms. Nevertheless, the staggered PRT velocity field displays velocity dealiasing errors.

3. DEALIASING ERRORS IN STAGGERED PRT

Some velocity dealiasing errors are expected in staggered PRT and plans to reduce these errors were implemented in the NEXRAD velocity dealiasing routine (Torres et al. 2009); subsequently, the ROC has since adopted a new velocity dealiasing algorithm (2DVDA). The use of the 2DVDA to improve the quality of the staggered PRT velocities was evaluated by a ROC internal blind study. Overall, the analysis concluded that 2DVDA improved the quality of the velocity field. However, further ROC analysis uncovered reduced performance of 2DVDA in the presence of staggered PRT dealiasing errors for some weather events such as clear air returns near the radar, weak echo returns on the fringes of stratiform events, strong echoes in squall lines, and storm top divergence near the end of the unambiguous range of the shorter PRT. It became obvious that these dealiasing errors required treatment at an earlier stage in the signal processing chain where some critical information could be obtained.

Our initial signal processing approach used the smoothed (3 to 7 range-gate running average) velocity estimates (i.e.: from the lag-1 autocorrelations short-to-

long v_1 and long-to-short v_2 PRTs) as input into the VDTF (Gray et al. 1989). Fig. 7 shows the velocity fields from a widespread stratiform rain event captured on the WSR-88D testbed KOUN on October 30, 2015. The left panel velocity field is normally processed using the VDTF to dealias v_1 while the right panel is processed using a running mean on the two velocity estimates before applying the VDTF to dealias the smoothed v_1. The red circles delineate the regions of primary concern displaying velocity dealiasing errors. It can be seen in the large red circle to the north of the radar that most of the dealiasing errors are corrected; however, clustering of errors appear at the fringes of the velocity field. The most egregious example of clustering is highlighted by the small red circle to the southwest of the radar. This method proved to reduce errors, but caused unacceptable clustering of bad velocities.

Our second approach (here out called 1DVDA) proved to be more effective. In this approach, we process each radial initially by dealiasing v_1 into the extended Nyquist co-interval with the appropriate solution from the VDTF (i.e. normal processing). Additionally, we monitor the fit of the velocity difference ($v_1 - v_2$) with the VDTF. That is, the VDTF using a 2/3 ratio has 5 unique values spaced $v_a/3$ apart where v_a is the extended Nyquist. Moreover, the velocity difference should match one of these unique values; however, errors in the velocity estimates (assumed Gaussian) create errors in the dealiased velocity. Consequently, the closeness of the fit is closely related to the velocity difference variance (Torres et al. 2004). If the velocity difference fits the VDTF closely (i.e., low variance), we flag it. If at least five sequential range-gates are flagged, we identify this set of gates as being verified with high confidence. This process is summarized in Fig. 8 where the velocity difference (top), VDTF (middle), difference between the velocity difference and the VDTF (bottom) are shown for 0.25° radial of the widespread stratiform rain event in Fig. 7 (left panel) as a function of range bins. The threshold (green line) delineates the high-confident region from the non-confident region.

A second pass (a continuity check) on the radial identifies regions of 5 or more sequential gates that have gate-to-gate circular differences (i.e., the minimum difference between velocity estimates when aliased on the Nyquist velocity co-interval) that are the same for both the v_1 estimate and the dealiased velocity. Additionally, these gates cannot have large shears (Zhang and Wang 2006, Eq. 2) in v_1 or v_2. We identify this set of gates as moderately confidence. Currently, we do not process the highly- and moderately-confident gates differently. The flags of the highly-confident and moderately-confident gates are combined to create a single confidence flag for each range gate (i.e., either highly- or moderately-confident flag = confident flag). Gates with these confidence flags will not be changed in the supplementary processing of the radial.

In the last pass, we attempt to correct the velocity errors in regions that are between confidence regions to reduce the circular difference between the velocity of the gate being processed and a reference velocity (5-gate mean obtained from the confidence regions). This

is accomplished by adding or subtracting the Nyquist velocity of the short PRT to the current dealiased velocity being processed (Note: This correction is specific to 2/3 staggered PRT). Regions at the beginning and end of a radial are processed with reference to the local (within 10 km) confidence region. All gates that are not locally close to a confidence region are not changed from the original VDTF solution. Fig. 9 shows the velocity fields from the same case as in Fig. 7. The left panel velocity field is normally processed with the VDTF while the right panel is processed with the addition of the 1DVDA algorithm. As can be seen in the right panel of Fig. 9, the velocity dealiasing errors have been significantly reduced. For this case, the normally processed velocity (left panel) with just the VDTF had ~2.43% velocity errors where the signal was not censored (either by SNR or Overlaid thresholds) while the 1DVDA (right panel) has reduced the errors down to less than a few hundredths of a percent (~0.03%). That is, about 97.5% of the errors were corrected using 1DVDA with no clustering of velocity errors. Residual errors are addressed by further processing using the 2DVDA algorithm. Testing has shown that this combined approach mitigates velocity dealiasing errors associated staggered PRT. For more examples and details, the reader is referred to the associated poster (Warde et al. 2019) that supplements this paper.

3. SUMMARY

The implementation and integration and some results of testing staggered PRT on the NEXRAD WSR-88D testbed have been presented. The analysis of staggered PRT output has shown improvement in the quality of reflectivity, spectrum width, differential reflectivity, cross-correlation coefficient, and differential phase over batch output. Furthermore, the unexpected increase in dealiasing errors associated with the staggered PRT waveform is mitigated using 1DVDA to identify and correct these errors. Although testing is not complete, the addition of 1DVDA will provide improved quality in the staggered PRT velocity.

4. ACKNOWLEDGEMENTS

6. REFEERENCES

Meymaris, G. and J. Hubbert, 2015. Hybrid Spectrum Width Estimator for Staggered PRT. Draft NCAR Report, 6 pp.

Meymaris, G., J. Williams, and J. Hubbert, 2009: An improved hybrid spectrum width estimator. *Proc. 34th Conf. on Radar Meteorology*, Williamsburg, VA, AMS, P5.20, 9 pp

Torres, S. M., Y. F. Dubel, and D. S. Zrnić, 2004: Design, Implementation, and demonstration of a staggered PRT algorithm. *J. Atmos. Oceanic Technol.*, **21**, 1389-1399

Torres, S., D. Zittel and D. Saxion, 2009: Update on deployment of staggered PRT for the NEXRAD network. *Preprints 25th Conf. on IIPS for Meteorology, Oceanography, and Hydrology*, Phoenix, AZ, Amer. Metoer. Soc., 11B.2, 6 pp.

Torres, S., and D. Warde, 2017: Staggered-PRT sequences for Doppler weather radars. Part I: Spectral analysis using the autocorrelation spectral density. *J. Atmos. Oceanic Technol.*, **34**, 51–63, doi:10.1175/JTECH-D-16-0071.1.

Warde, D. A., and S. Torres, 2009: The Range-Overlaid Staggered PRT Algorithm. Preprints, *34th International Conference on Radar Meteorology*, Williamsburg, VA, USA, Amer. Metoer. Soc., P5.11, 6 pp.

Warde, D. A., and S. M. Torres, 2014: Improved spectrum width estimators for Doppler weather radars. Preprints, *8th European Conf. on Radar in Meteor. and Hydrology (ERAD)*, Garmisch-Partenkirchen, Germany, Deutscher Wetterdienst and Deutsches Zentrum für Luft- und Raumfahrt, P10, 8 pp.

Warde, D. and S. Torres, 2017a: Staggered-PRT Sequences for Doppler Weather Radars. Part II: Ground Clutter Mitigation on the NEXRAD Network Using the CLEAN-AP Filter. *J. Atmos. Oceanic Technol.*, **34**, 703–716, doi:10.1175/JTECH-D-16-0072.1.

Warde D. and S. Torres, 2017b: Spectrum Width Estimation Using Matched Autocorrelations. *IEEE Geosci. Remote Sens. Lett.*, **14**, 1661–1664, doi: 10.1109/LGRS.2017.2726898.

Warde, D., A. Heck, J. Krauss, A. Losey, and W. D. Zittel, 2019: A Novel Approach to Reducing

Dealiasing Errors for Staggered Pulse Repetition Time Waveforms. *35ᵗʰ Conf. on Environmental Information Processing Technologies*, Phoenix, AZ, Amer. Metoer. Soc., Poster 828.
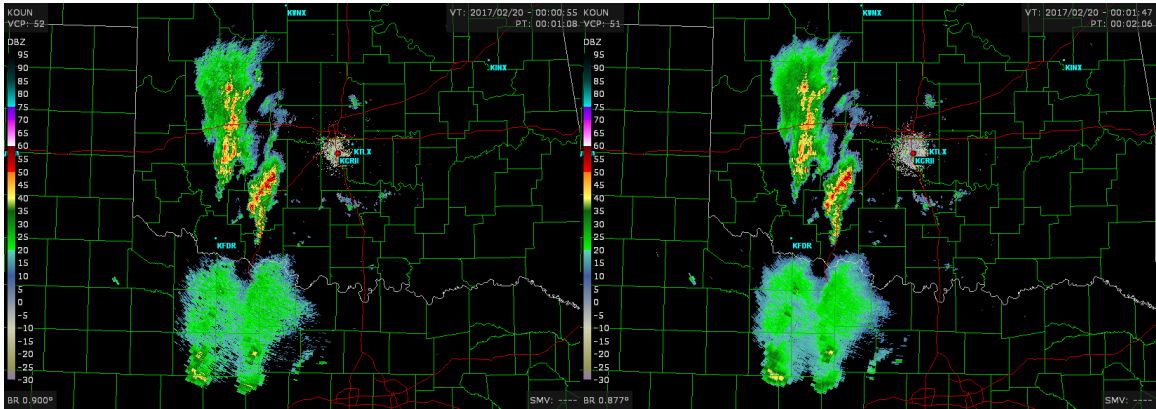

Figure 1. Reflectivity PPI at 0.9° elevation from batch (left) and staggered PRT (right).
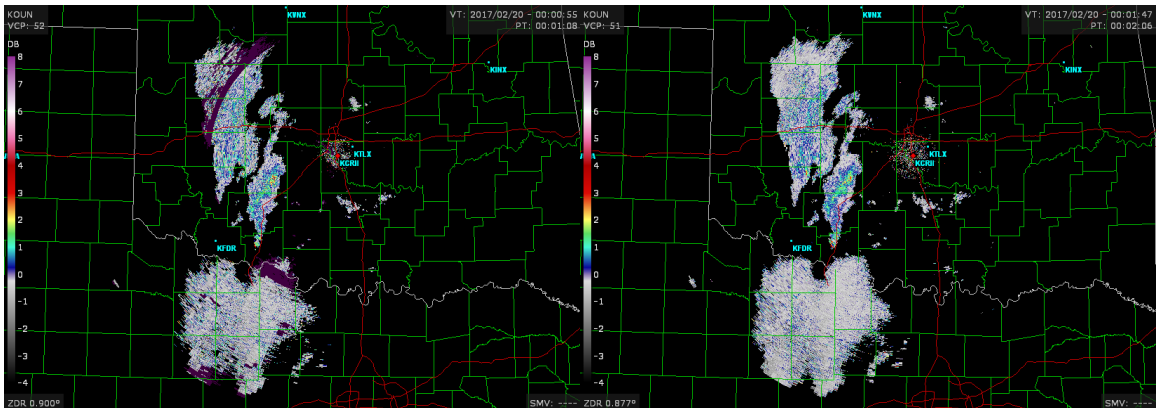

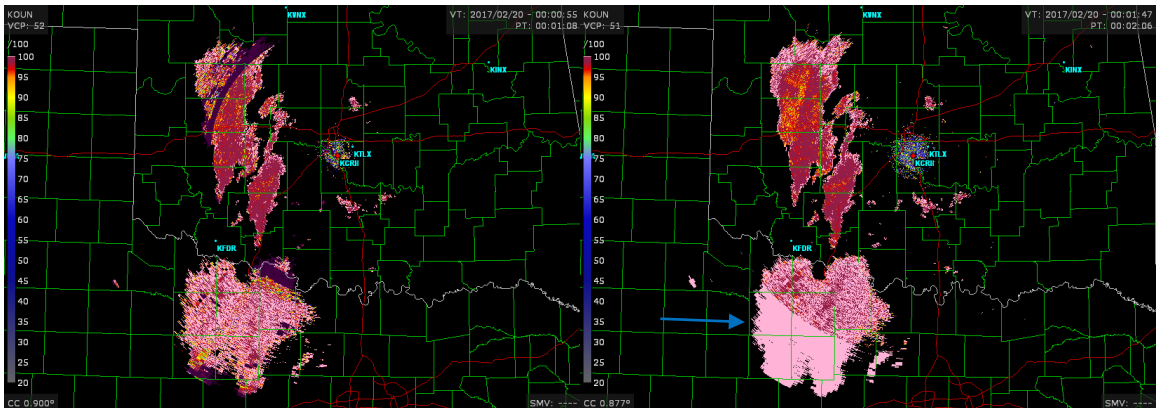**Figure 2. Differential Reflectivity PPI at 0.9° elevation from batch (left) and staggered PRT (right).**

Figure 3. Correlation Coefficient PPI at 0.9° elevation from batch (left) and staggered PRT (right). Note: Blue arrow points to a region that displays incorrect values found and corrected during the validation process.
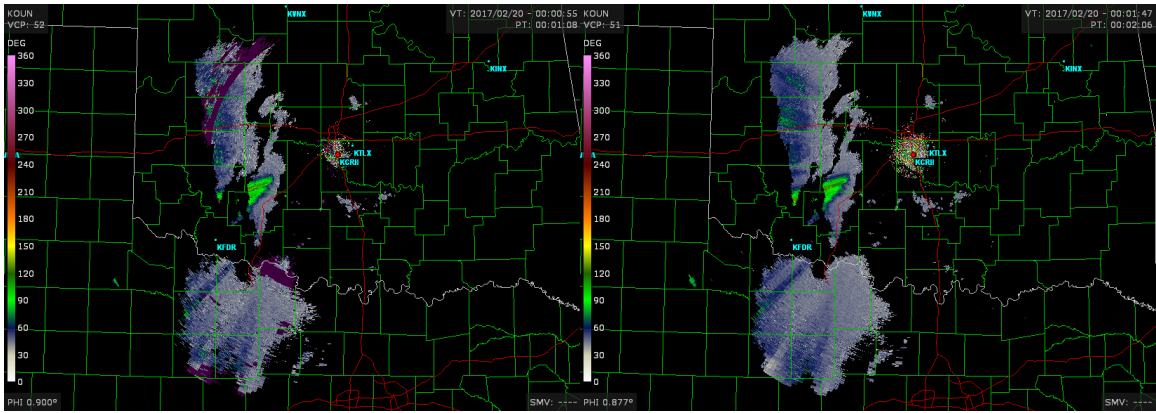
Figure 4. Differential Phase PPI at 0.9° elevation from batch (left) and staggered PRT (right).
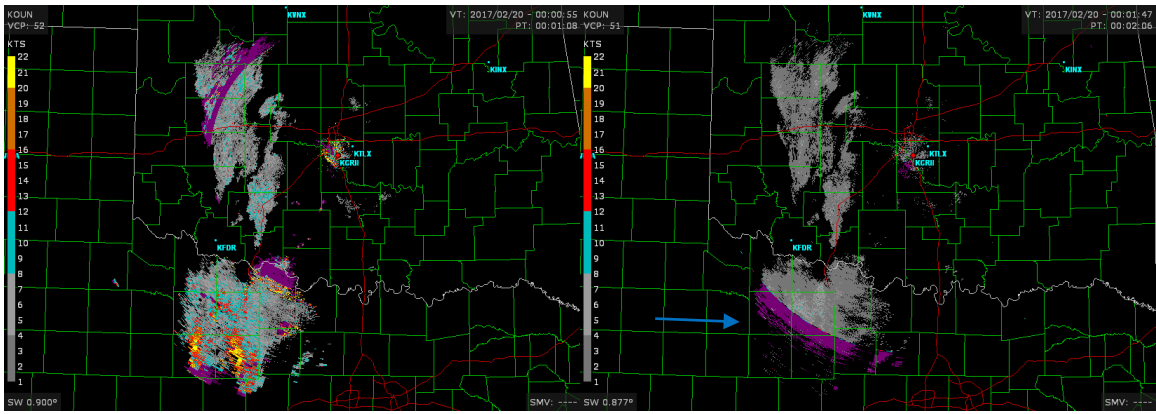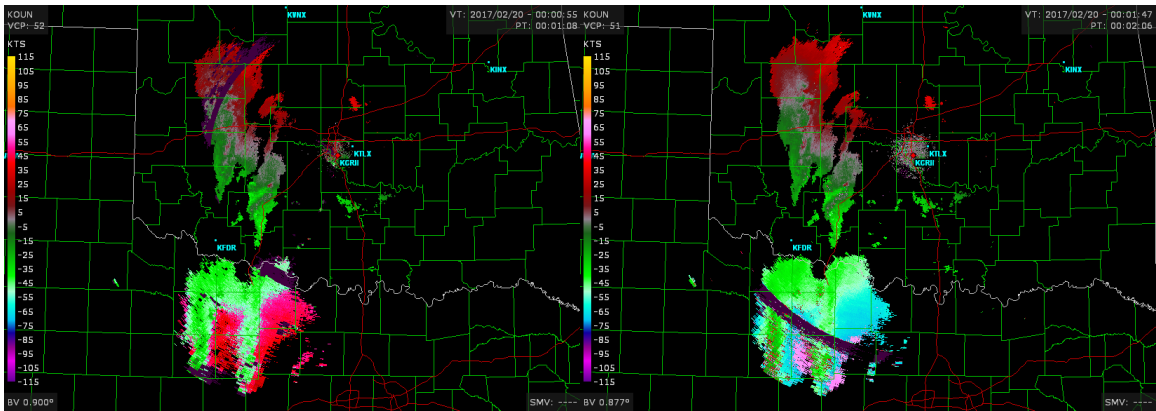

Figure 5. Spectrum Width PPI at 0.9° elevation from batch (left) and staggered PRT (right). Note: Blue arrow points to a region that displays incorrect values found and corrected during the validation process.

Figure 6. Velocity PPI at 0.9° elevation from batch (left) and staggered PRT (right).
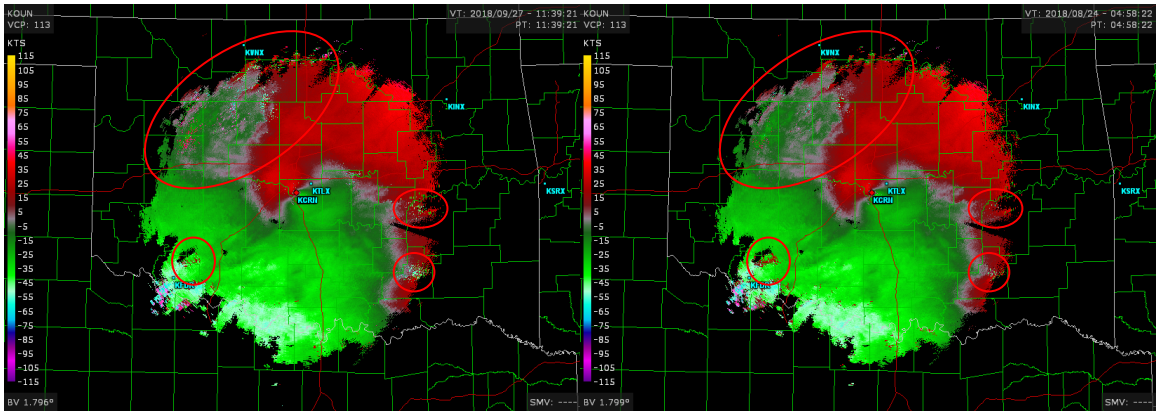
Fig. 7. Velocity PPI at 1.8° elevation from staggered PRT using VDTF normal processing (left) and smoothed processing (right). Red circles indicate regions where dealiasing errors occur.
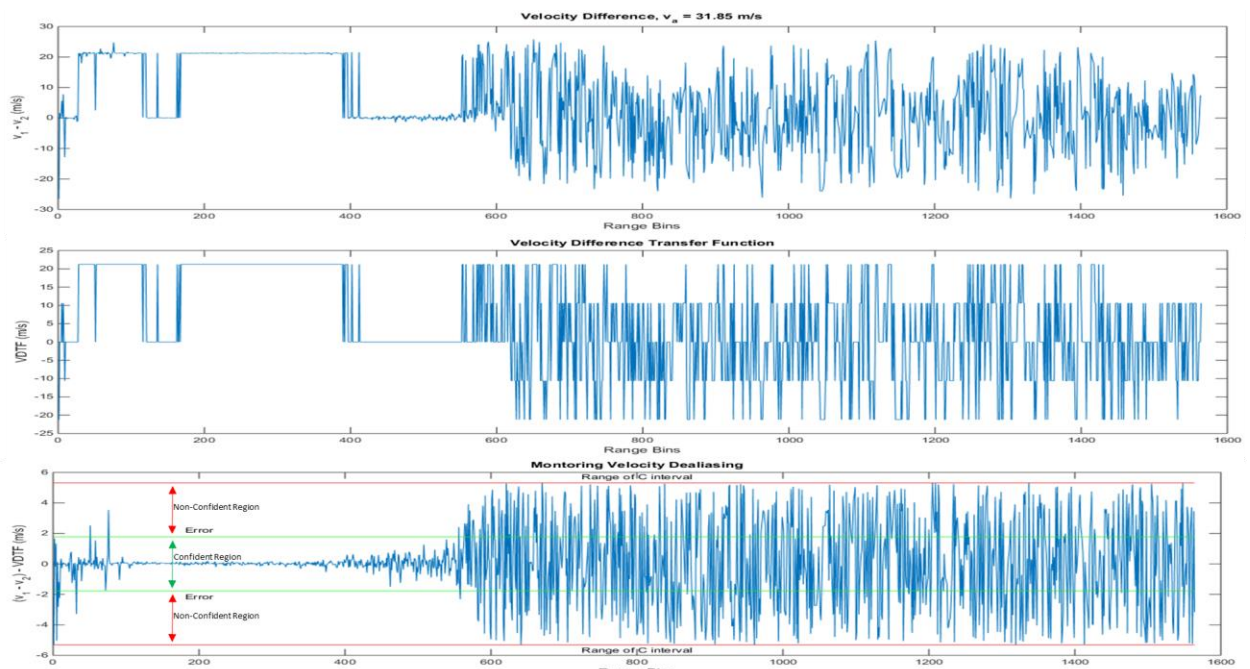

Fig. 8. Monitoring Dealiasing Errors, radial (0.25° Az.) of widespread rain case shown in Fig. 7 (left panel)
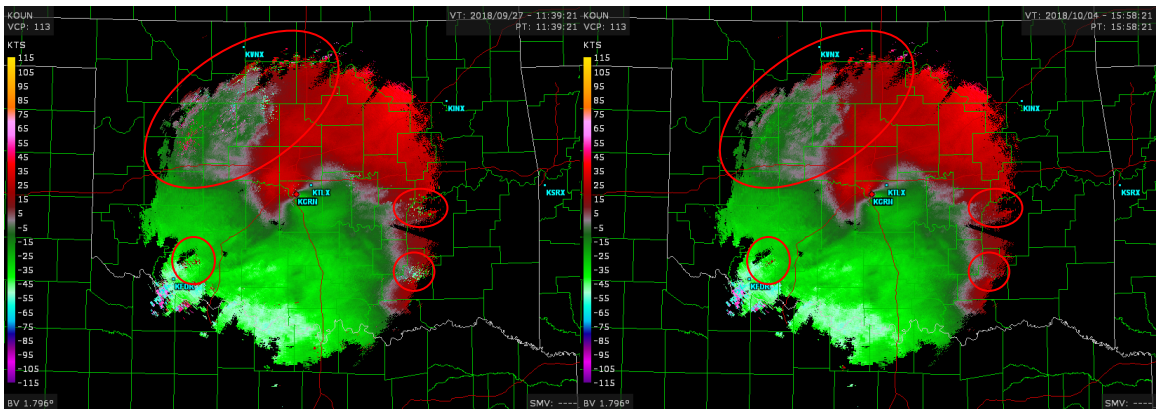

Fig. 9. Velocity PPI at 1.8° elevation from staggered PRT using VDTF normal processing (left) and VDTF&1DVDA processing (right). Red circles indicate regions where dealiasing errors occur.